

Sequential Conditional Transport on Probabilistic Graphs for Interpretable Counterfactual Fairness

Agathe Fernandes Machado^{✉1}, Arthur Charpentier¹, and Ewen Gallic²

¹Département de Mathématiques, Université du Québec à Montréal, Montréal, Québec, Canada

²Aix Marseille Univ, CNRS, AMSE, Marseille, France

August 8, 2024

Abstract

In this paper, we link two existing approaches to derive counterfactuals: adaptations based on a causal graph, as suggested in [Plečko and Meinshausen \(2020\)](#) and optimal transport, as in [De Lara et al. \(2024\)](#). We extend “Knothe’s rearrangement” [Bonnotte \(2013\)](#) and “triangular transport” [Zech and Marzouk \(2022a\)](#) to probabilistic graphical models, and use this counterfactual approach, referred to as sequential transport, to discuss individual fairness. After establishing the theoretical foundations of the proposed method, we demonstrate its application through numerical experiments on both synthetic and real datasets.

1 Introduction

Most applications concerning discrimination and fairness are based on “group fairness” concepts (as introduced in [Hardt, Price, and Srebro \(2016\)](#); [Kearns and Roth \(2019\)](#), or [Barocas, Hardt, and Narayanan \(2023\)](#)). However, in many applications, fairness should be addressed at the individual level rather than globally. As claimed in [Dwork et al. \(2012\)](#), “*we capture fairness by the principle that any two individuals who are similar with respect to a particular task should be classified similarly.*” The concept of “counterfactual fairness” was formalized in [Kusner et al. \(2017\)](#), addressing questions such as “*had the protected attributes of the individual been different, other things being equal, would the decision had remain the same?*” Such a statement has clear connections with causal inference, as discussed in [Pearl and Mackenzie \(2018\)](#). Formally, consider observations $\{s_i, \mathbf{x}_i, y_i\}$, where s is a binary protected attribute (e.g., $s \in \{0, 1\}$), and \mathbf{x} is a collection of legitimate features (possibly correlated with s). The model output is y , which is analyzed to address “algorithmic fairness” issues. Following [Rubin \(2005\)](#), let $y^*(s)$ denote the potential outcome of y if s is seen as a treatment. With these notations, counterfactual fairness is achieved, for individual (s, \mathbf{x}) if the average “treatment effect,” conditional on \mathbf{x} (coined “CATE”) is zero, i.e., $\mathbb{E}[Y^*(1) - Y^*(0) | \mathbf{X} = \mathbf{x}] = 0$. This quantity could be termed

Ewen Gallic acknowledge that the project leading to this publication has received funding from the French government under the “France 2030” investment plan managed by the French National Research Agency (reference: ANR-17-EURE-0020) and from Excellence Initiative of Aix-Marseille University—A*MIDEX.

Replication codes and companion e-book: https://github.com/fer-agathe/sequential_transport

✉Corresponding author: fernandes_machado.agathe@courrier.uqam.ca

“*ceteris paribus* CATE” since all \mathbf{x} ’s are supposed to remain unchanged, for both treated and non-treated individuals.

Following [Kilbertus et al. \(2017\)](#), it is possible to suppose that the protected attribute s could actually affect some explanatory variables \mathbf{x} in a non-discriminatory way. In [Charpentier, Flachaire, and Gallic \(2023\)](#), the outcome y was “having a surgical intervention” during childbirth in the U.S., s was the mother’s ethnic origin (“Black,” or not) and \mathbf{x} included factors such as “weight of the baby at birth.” If Black mothers undergo less surgery because they tend to have smaller babies, there is no discrimination *per se*. At the very least, it should be fair, when assessing whether hospitals have discriminatory policies, to account for that difference in baby weights. Such a variable is named “revolving variable” in [Kilbertus et al. \(2017\)](#). Using heuristic notations, the “*ceteris paribus* CATE” $\mathbb{E}[Y^*(1)|\mathbf{X} = \mathbf{x}] - \mathbb{E}[Y^*(0)|\mathbf{X} = \mathbf{x}]$ should become a “*mutatis mutandis* CATE”. For some individual ($s = 0, \mathbf{x}$), this indicator would be $\mathbb{E}[Y^*(1)|\mathbf{X} = \mathbf{x}^*(1)] - \mathbb{E}[Y^*(0)|\mathbf{X} = \mathbf{x}]$, as coined in [Charpentier, Flachaire, and Gallic \(2023\)](#), to quantify discrimination, where fictitious individual ($s = 1, \mathbf{x}^*(1)$) is a “counterfactual” version of ($s = 0, \mathbf{x}$).

Two recent approaches have been proposed to assess counterfactual fairness using this *mutatis mutandis* approach. On the one hand, [Plečko and Meinshausen \(2020\)](#) and [Plečko, Bennett, and Meinshausen \(2021\)](#) used causal graphs (DAGs) to construct counterfactuals and assess the counterfactual fairness of outcomes y based on variables (s, \mathbf{x}, y) . In network flow terminology, s acts as a “source” (only outgoing flow, or no parents), while y is a “sink” (only incoming flow). On the other hand, [Charpentier, Flachaire, and Gallic \(2023\)](#) and [De Lara et al. \(2024\)](#) used optimal transport (OT) to construct counterfactuals. While [De Lara et al. \(2024\)](#) provided a theoretical framework, its implementation is challenging (except in the Gaussian case), and usually hard to interpret. Here, we combine the two approaches, using OT within a causal graph structure. The idea is to adapt “Knothe’s rearrangement” [Bonnotte \(2013\)](#), or “triangular transport” [Zech and Marzouk \(2022a,b\)](#), to a general probabilistic graphical model on (s, \mathbf{x}, y) , rather than a simplistic $s \rightarrow x_1 \rightarrow x_2 \rightarrow \dots \rightarrow x_d \rightarrow y$. The concept of “conditional optimal transport” has been recently discussed in [Bunne, Krause, and Cuturi \(2022\)](#) and [Hosseini, Hsu, and Taghvaei \(2023\)](#), but here, instead of learning the causal graph, we assume a known causal graph and use it to construct counterfactual versions of individuals (s_i, \mathbf{x}_i, y_i) to address fairness issues. Additionally, since we use univariate (conditional) transport, standard classical properties of univariate transport facilitates explanations (non-decreasing mappings, and quantile based interpretations).

Main Contributions

- We leverage multivariate transport theory for constructing counterfactuals, as suggested in [De Lara et al. \(2024\)](#), and connect it to quantile preservation on causal graphs from [Plečko and Meinshausen \(2020\)](#) to develop a sequential transport methodology that aligns with the underlying DAG of the data.
- Sequential transport, using univariate transport maps, provides closed-form solutions for deriving counterfactuals. This allows for the development of a data-driven estimation procedure that can be applied to new out-of-samples observations without recalculating, unlike multivariate OT with non-Gaussian distributions.
- The approach’s applicability is demonstrated through numerical experiments on both a synthetic dataset and a case study, highlighting the interpretable analysis of individual counterfactual fairness when using sequential transport.

Section 2 introduces various concepts used in probabilistic graphical models from a causal perspective. Section 3, revisits classical optimal transport covering both univariate and multivariate cases. Sequential transport is covered in Section 4. Section 5 discusses counterfactual fairness. Illustration with real data are provided in Section 6. Section 7 concludes.

2 Graphical Model and Causal Network

2.1 Probabilistic Graphical Model

Following standard notations in probabilistic graphical models (see [Koller and Friedman \(2009\)](#) or [Barber \(2012\)](#)), given a random vector $\mathbf{X} = (X_1, \dots, X_d)$, consider a directed acyclic graph (DAG) $\mathcal{G} = (V, E)$, where $V = \{x_1, x_2, \dots, x_d\}$ are the vertices (corresponding to each variable), and E are directed edges, such that $x_i \rightarrow x_j$ means “variable x_i causes variable x_j ,” in the sense of [Susser \(1991\)](#). The joint distribution of \mathbf{X} satisfies the (global) Markov property w.r.t. \mathcal{G} :

$$\mathbb{P}[x_1, \dots, x_d] = \prod_{j=1}^d \mathbb{P}[x_j | \text{parents}(x_j)],$$

where $\text{parents}(x_i)$ are nodes with edges directed towards x_i , in \mathcal{G} . [Watson et al. \(2021\)](#) suggested the causal graph in Figure 1 for the German Credit dataset, where s is the “sex” (top left) and y is the “default” indicator (right). Observe that variables x_j are here sorted. As discussed in [Ahuja, Magnanti, and Orlin \(1993\)](#), such a causal graph imposes some ordering on variables. In this “topological sorting,” a vertex must be selected before its adjacent vertices, which is feasible because each edge is directed such that no cycle exists in the graph. In our analysis, we consider a network \mathcal{G} on variables $\{s, x, y\}$ where s is the sensitive attribute, acting as a “source” (only outgoing flow, or no parents) while y is a “sink” (only incoming flow, i.e., $y \notin \text{parents}(x_i), \forall i$).

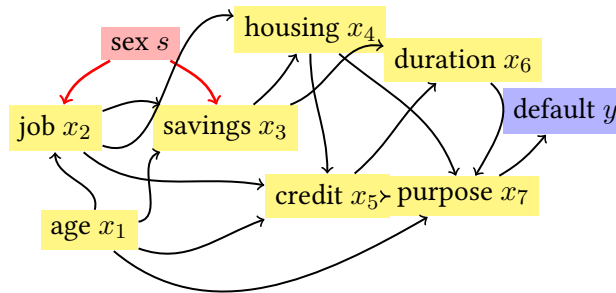


Figure 1: Causal graph in the German Credit dataset from [Watson et al. \(2021\)](#), or DAG.

2.2 Causal Networks and Structural Models

[Wright \(1921, 1934\)](#) used directed graphs to represent probabilistic cause-and-effect relationships among a set of variables and developed path diagrams and path analysis. Simple causal networks can be visualized on top of Figure 2. On the left is a simple model where the “cause” C directly causes (\rightarrow) the “effect” E . On the right, a “mediator” X is added. There is still the direct impact of C on E ($C \rightarrow E$), but there is also a mediated indirect impact ($C \rightarrow X \rightarrow E$).

2.2.1 Intervention in a Linear Structural Model

In a simple causal graph, with two nodes, C (the cause) and E (the effect), the causal graph is $C \rightarrow E$, and the mathematical interpretation can be summarized in two (linear) assignments:

$$\begin{cases} C = a_c + U_C \\ E = a_e + b_e C + U_E, \end{cases} \quad (1)$$

where U_C and U_E are independent Gaussian random variables. That causal graph can be visualized in Figure 2, and its corresponding structural causal model (SCM) described in Equation 1 illustrates the causal relationships between variables, as in Pearl (2000). Suppose here that C is a binary variable, taking values in $\{c_0, c_1\}$. Given an observation (c_0, e) , the ‘‘counterfactual outcome’’ if the cause had been set to c_1 (corresponding to the intervention in Figure 3), would be $e + b_e(c_1 - c_0)$.

2.2.2 Using a Twin Network

Following Pearl (2009), one can introduce the ‘‘twin network’’ shown in Figure 4, with the initial causal graph at the bottom, and a mirrored version (the twin causal graph) in the counterfactual world at the top. The idea is that the causal mapping $C \rightarrow E$ remains unchanged (we simply consider a different input value). Plečko and Meinshausen (2020) coined this approach ‘‘fair-twin projection’’ when C is a binary sensitive attribute, and the goal is to assess fairness in the effect E . In Figures 2–4, a mediator variable X is added on the right. Given the observation (c_0, x, e) , the counterfactual outcome associated with cause c_1 is e^* . By following the DAG in Figure 3, we can determine the effects of the do-intervention $\text{do}(C = c_1)$ through the pathways of X and E , using the observed data to estimate the error terms.

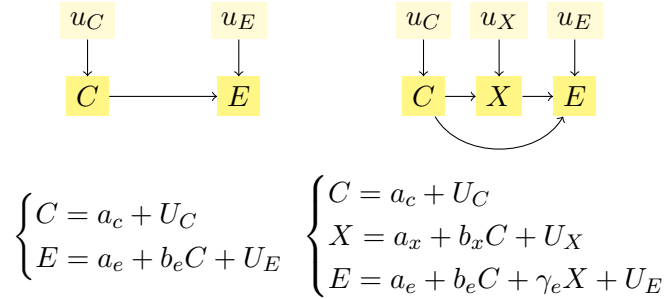


Figure 2: Linear Structural Causal Model – observation.

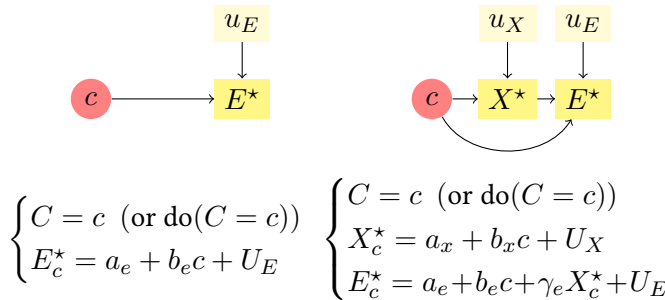


Figure 3: Linear Structural Causal Model – intervention.

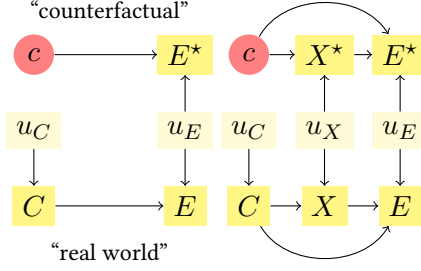


Figure 4: Structural Causal Model – twin network.

2.3 Non-Linear Structural Models

2.3.1 Presentation of the Model

More generally, consider a non-Gaussian and nonlinear structural model, named “non-parametric structural equation model” (with independent errors) in [Pearl \(2000\)](#),

$$\begin{cases} C = h_c(U_C) \\ E = h_e(C, U_E), \end{cases} \quad (2)$$

where $u \mapsto h_c(\cdot, u)$ and $u \mapsto h_e(\cdot, E)$ are strictly increasing in u ; U_C and U_E are independent, and, without loss of generality, supposed to be uniform on $[0, 1]$. For a rigorous mathematical framework for non-linear non-Gaussian structural causal models, see [Bongers et al. \(2021\)](#) or [Shpitser, Richardson, and Robins \(2022\)](#).

2.3.2 Connections With Conditional Quantiles

Consider now some general DAG, \mathcal{G} , on $\mathbf{X} = (X_1, \dots, X_d)$, supposed to be absolutely continuous. With previous notations, $X_i = h_i(\text{parents}(X_i), U_i)$, a.s., for all variables, representing the structural equations. We can write this compactly as $\mathbf{X} = h(\text{parents}(\mathbf{X}), \mathbf{U})$, a.s., by considering h as a vector function. Solving the structural model means finding a function g such that $\mathbf{X} = g(\mathbf{U})$, a.s. To illustrate, consider a specific i , and $X_i = h_i(\text{parents}(X_i), U_i)$. If $\text{parents}(X_i) = \mathbf{x}$ is fixed, define $h_{i|\mathbf{x}}(u) = h_i(\mathbf{x}, u)$. Let U be a uniform random variable, and let $F_{i|\mathbf{x}}$ be the cumulative distribution of $h_{i|\mathbf{x}}(U)$, $F_{i|\mathbf{x}}(x) = \mathbb{P}[h_{i|\mathbf{x}}(U) \leq x]$. Since X_i is absolutely continuous, $F_{i|\mathbf{x}}$ is invertible, and $F_{i|\mathbf{x}}^{-1}$ is a conditional quantile function (conditional on $\text{parents}(X_i) = \mathbf{x}$). Let $V = F_{i|\mathbf{x}}(h_{i|\mathbf{x}}(U))$, then $X_i = F_{i|\mathbf{x}}^{-1}(V)$ and V is uniformly distributed on $[0, 1]$. This means that x_i corresponds to the quantile of variable X_i , conditional on the values of its parents, $\text{parents}(X_i)$, with probability level u_i . In the mirror world of the “twin network” in [Figure 4](#), u_i represents the (conditional) probability level associated with observation x_i , and its counterfactual counterpart is x_i^* corresponding to the (conditional) quantile associated with the same probability level u_i .

This representation has been used in [Plečko and Meinshausen \(2020\)](#) and [Plečko, Bennett, and Meinshausen \(2021\)](#), where $X_i = F_{i|\mathbf{x}}^{-1}(V)$ is simply the probabilistic representation of “quantile regression,” as introduced by [Koenker and Bassett Jr \(1978\)](#) (and further studied in [Koenker \(2005\)](#) and [Koenker et al. \(2017\)](#)). This could be extended to “quantile regression forests,” as in [Meinshausen and Ridgeway \(2006\)](#), or any kind of machine learning model, as [Cannon \(2018\)](#) or [Pearce et al. \(2022\)](#). Observe that [Ma and Koenker \(2006\)](#) considered some close “recursive structural equation models,” characterized by a system of equations where each endogenous variable is regressed on other endogenous and exogenous variables in a hierarchical manner. They used some sequential quantile regression approach to solve those recursive SEMs. An alternative that we consider here is to use the connection between quantiles and

optimal transport (discussed in [Chernozhukov, Fernández-Val, and Melly \(2013\)](#) or [Hallin and Konen \(2024\)](#)) to define some “conditional transport” that relates to those conditional quantiles.

3 Optimal Transport

Given two metric spaces \mathcal{X}_0 and \mathcal{X}_1 , consider a measurable map $T : \mathcal{X}_0 \rightarrow \mathcal{X}_1$ and a measure μ_0 on \mathcal{X}_0 . The push-forward of μ_0 by T is the measure $\mu_1 = T_{\#}\mu_0$ on \mathcal{X}_1 defined by $T_{\#}\mu_0(B) = \mu_0(T^{-1}(B))$, $\forall B \subset \mathcal{X}_1$. For all measurable and bounded $\varphi : \mathcal{X}_1 \rightarrow \mathbb{R}$,

$$\int_{\mathcal{X}_1} \varphi(x_1) T_{\#}\mu_0(dx_1) = \int_{\mathcal{X}_0} \varphi(T(x_0)) \mu_0(dx_0).$$

For our applications, if we consider measures $\mathcal{X}_0 = \mathcal{X}_1$ as a compact subset of \mathbb{R}^d , then there exists T such that $\mu_1 = T_{\#}\mu_0$, when μ_0 and μ_1 are two measures, and μ_0 is atomless, as shown in [Villani \(2003\)](#) and [Santambrogio \(2015\)](#). In that case, and if we further suppose that measures μ_0 and μ_1 are absolutely continuous, with densities f_0 and f_1 (w.r.t. Lebesgue measure), a classical change of variable expression can be derived. Specifically, the previous integral

$$\int_{\mathcal{X}_1} \varphi(\mathbf{x}_1) f_1(\mathbf{x}_1) d\mathbf{x}_1$$

is simply (if ∇T is the Jacobian matrix of mapping T):

$$\int_{\mathcal{X}_0} \varphi(T(\mathbf{x}_0)) \underbrace{f_1(T(\mathbf{x}_0)) \det \nabla T(\mathbf{x}_0)}_{=f_0(\mathbf{x}_0)} d\mathbf{x}_0.$$

Out of those mappings from μ_0 to μ_1 , we can be interested in “optimal” mappings, satisfying Monge problem, from [Monge \(1781\)](#), i.e., solutions of

$$\inf_{T_{\#}\mu_0=\mu_1} \int_{\mathcal{X}_0} c(\mathbf{x}_0, T(\mathbf{x}_0)) \mu_0(d\mathbf{x}_0),$$

for some positive ground cost function $c : \mathcal{X}_0 \times \mathcal{X}_1 \rightarrow \mathbb{R}_+$.

In general settings, however, such a deterministic mapping T between probability distributions may not exist (in particular if μ_0 and μ_1 are not absolutely continuous, with respect to Lebesgue measure). This limitation motivates the Kantorovich relaxation of Monge’s problem, as considered in [Kantorovich \(1942\)](#),

$$\inf_{\pi \in \Pi(\mu_0, \mu_1)} \int_{\mathcal{X}_0 \times \mathcal{X}_1} c(\mathbf{x}_0, \mathbf{x}_1) \pi(d\mathbf{x}_0, d\mathbf{x}_1),$$

with our cost function c , where $\Pi(\mu_0, \mu_1)$ is the set of all couplings of μ_0 and μ_1 . This problem focuses on couplings rather than deterministic mappings. It always admits solutions referred to as optimal transport plans.

3.1 Univariate Optimal Transport

Suppose here that $\mathcal{X}_0 = \mathcal{X}_1$ is a compact subset of \mathbb{R} . The optimal Monge map T^* for some strictly convex cost c such that $T_{\#}^*\mu_0 = \mu_1$ is $T^* = F_1^{-1} \circ F_0$, where $F_i : \mathbb{R} \rightarrow [0, 1]$ is the cumulative distribution function associated with μ_i , $F_i(x) = \mu_i((-\infty, x])$, and F_i^{-1} is the generalized inverse (corresponding to the quantile function), $F_i^{-1}(u) = \inf \{x \in \mathbb{R} : F_i(x) \geq u\}$. Observe that T^* is an increasing mapping (which is the univariate definition of being the gradient of a convex function, from [Brenier \(1991\)](#)). This can be visualized in [Figure 5](#), with a Gaussian case on the left (T^* is then affine), and with general densities on the right.

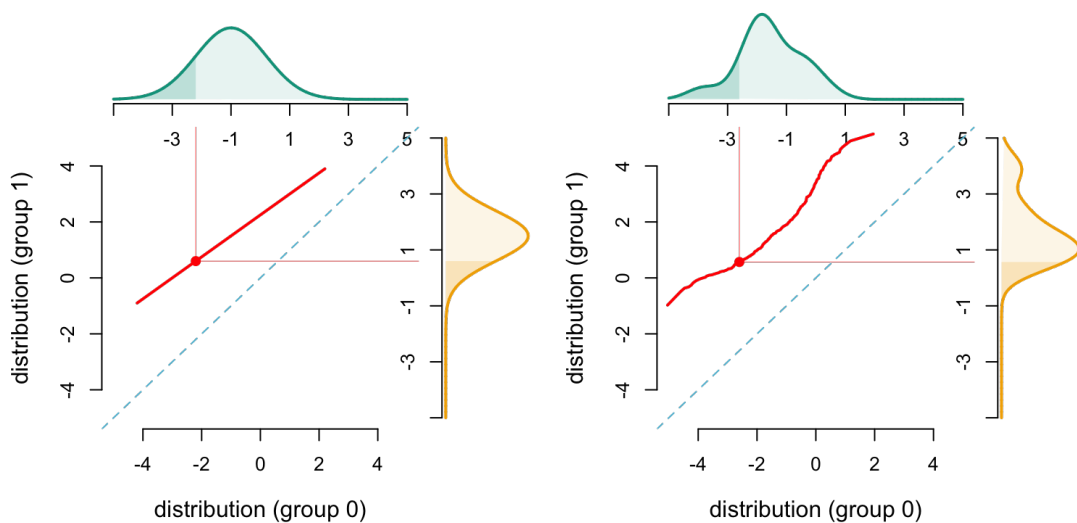


Figure 5: Univariate optimal transport, with Gaussian distributions (left) and general marginal distributions (right). The transport curve (T^*) is shown in red.

3.2 Multivariate Optimal Transport

In a multivariate setting, when $\mathcal{X}_0 = \mathcal{X}_1$ is a compact subset of \mathbb{R}^d , from [Brenier \(1991\)](#), with a quadratic cost, the optimal Monge map T^* is unique, and it is the gradient of a convex mapping $\psi : \mathbb{R}^d \rightarrow \mathbb{R}^d$, $T^* = \nabla\psi$. Therefore, its Jacobian matrix ∇T^* is nonnegative and symmetric. More generally, with strictly convex cost in $\mathbb{R}^d \times \mathbb{R}^d$, the Jacobian matrix ∇T^* , even if not necessarily nonnegative symmetric, is diagonalizable with nonnegative eigenvalues, as proved in [Cordero-Erausquin \(2004\)](#) and [Ambrosio, Gigli, and Savaré \(2005\)](#). Unfortunately, it is generally difficult to give an analytic expression for the optimal mapping T^* , unless additional assumptions are made, such as assuming that both distributions are Gaussian, as in [Appendix A](#).

4 Sequential Transport

4.1 Knothe-Rosenblatt Conditional Transport

As explained in [Villani \(2003\)](#); [Carlier, Galichon, and Santambrogio \(2010\)](#); [Bonnotte \(2013\)](#), the Knothe-Rosenblatt rearrangement is directly inspired by the Rosenblatt chain rule, from [Rosenblatt \(1952\)](#), and some extensions obtained on general measures by [Knothe \(1957\)](#). Using notations of Section 2.3 in [Santambrogio \(2015\)](#), suppose that the measure μ_0 is absolutely continuous on \mathbb{R}^d , and let $\mu_{0:d}$ denote the marginal d -th measure, $\mu_{0:d-1|d}$ the conditional $d-1$ -th measure (given x_d), $\mu_{0:d-2|d-1,d}$ the conditional $d-2$ -th measure (given x_{d-1} and x_d), etc. For the first two,

$$\begin{aligned} \mu_0(\mathbb{R}^{d-1} \times dx_d) &= \mu_{0:d}(dx_d) \\ \mu_0(\mathbb{R}^{d-2} \times dx_{d-1} \times dx_d) &= \mu_{0:d}(dx_d)\mu_{0:d-1|d}(dx_{d-1}|x_d) \end{aligned}$$

and iterate. Define conditional (univariate) cumulative distribution functions:

$$\begin{cases} F_{0:d}(x_d) = \mu_{0:d}((-\infty, x_d]) = \mu_0(\mathbb{R}^{d-1} \times (-\infty, x_d]) \\ F_{0:d-1|d}(x_{d-1}|x_d) = \mu_{0:d-1|d}((-\infty, x_{d-1}]|x_d), \end{cases}$$

etc. And similarly for μ_1 . For the first component, let T_d^* denote the monotone nondecreasing map transporting from $\mu_{0:d}$ to $\mu_{1:d}$, defined as $T_d^*(\cdot) = F_{1:d}^{-1}(F_{0:d}(\cdot))$. For the second component, let $T_{d-1}^*(\cdot|x_d)$ denote the monotone nondecreasing map transporting from $\mu_{0:d-1|d}(\cdot|x_d)$ to $\mu_{1:d-1|d}(\cdot|T_d^*(x_d))$, $T_{d-1}^*(\cdot|x_d) = F_{1:d-1|d}^{-1}(F_{0:d-1|d}(\cdot|x_d)|T_d^*(x_d))$. We can then repeat the construction, and finally, the Knothe-Rosenblatt rearrangement is

$$T_{\overline{kr}}(x_1, \dots, x_d) = \begin{pmatrix} T_1^*(x_1|x_2, \dots, x_d) \\ T_2^*(x_2|x_3, \dots, x_d) \\ \vdots \\ T_{d-1}^*(x_{d-1}|x_d) \\ T_d^*(x_d) \end{pmatrix}.$$

As proved in Santambrogio (2015) and Carlier, Galichon, and Santambrogio (2010), $T_{\overline{kr}}$ is a transportation map from μ_0 to μ_1 , in the sense that $\mu_1 = T_{\overline{kr}\#}\mu_0$. Following Bogachev, Kolesnikov, and Medvedev (2005), $T_{\overline{kr}}$ is the ‘‘monotone upper triangular map,’’ and it is unique. Bogachev, Kolesnikov, and Medvedev (2005) defined the ‘‘monotone lower triangular map,’’

$$T_{\underline{kr}}(x_1, \dots, x_d) = \begin{pmatrix} T_1^*(x_1) \\ T_2^*(x_2|x_1) \\ \vdots \\ T_{d-1}^*(x_{d-1}|x_1, \dots, x_{d-2}) \\ T_d^*(x_d|x_1, \dots, x_{d-1}) \end{pmatrix}.$$

The map $x_i \mapsto T_i^*(x_i|x_1, \dots, x_{i-1})$ is monotone (nondecreasing) for all $(x_1, \dots, x_{i-1}) \in \mathbb{R}^{i-1}$. Further, by construction, this Knothe-Rosenblatt transport map has a triangular Jacobian matrix $\nabla T_{\underline{kr}}$ with nonnegative entries on its diagonal, making it suitable for various geometric applications. However, this mapping does not satisfy many properties; for example, it is not invariant under isometries of \mathbb{R}^d as mentioned in Villani (2009). Carlier, Galichon, and Santambrogio (2010) proved that the Knothe-Rosenblatt transport maps could be seen as limits of quadratic optimal transports. A direct interpretation is that this iterative sequential transport can be seen as ‘‘marginally optimal.’’ Some explicit formulas can be obtained in the Gaussian case, as discussed in Appendix A.

4.2 Sequential Conditional Transport on a Probabilistic Graph

The ‘‘monotone lower triangular map,’’ introduced in Bogachev, Kolesnikov, and Medvedev (2005) could be used when dealing with time series, since there is a natural ordering between variables, indexed by the time, as discussed in Backhoff et al. (2017) or Bartl, Beiglböck, and Pammer (2021). In the general non-temporal case of time series X_t , it is natural to extend that approach to acyclical probabilistic graphic models, following Cheridito and Eckstein (2023). Instead of two general measures μ_0 and μ_1 on \mathbb{R}^d , we use only measures ‘‘factorized according to \mathcal{G} ,’’ some probabilistic graphical model, as defined in Lauritzen (2020).

Definition. Consider some acyclical causal graph \mathcal{G} on (s, \mathbf{x}) where variables are topologically sorted, where $s \in \{0, 1\}$ is a binary variable, defining two measures μ_0 and μ_1 on \mathbb{R}^d , by condi-

tioning on $s = 0$ and $s = 1$, respectively, factorized according to \mathcal{G} . Define

$$T_{\mathcal{G}}^*(x_1, \dots, x_d) = \begin{pmatrix} T_1^*(x_1) \\ T_2^*(x_2 | \text{parents}(x_2)) \\ \vdots \\ T_{d-1}^*(x_{d-1} | \text{parents}(x_{d-1})) \\ T_d^*(x_d | \text{parents}(x_d)) \end{pmatrix}.$$

This mapping will be called “sequential conditional transport on the graph \mathcal{G} .”

A classical algorithm for topological sorting is [Kahn \(1962\)](#)’s “Depth First Search” (DFS), and other algorithms are discussed in Section 20.4 in [Cormen et al. \(2022\)](#). For the causal graphs of Figure 6:

$$T_{\mathcal{G}}^*(x_1, x_2) = \begin{pmatrix} T_1^*(x_1) \\ T_2^*(x_2 | x_1) \end{pmatrix}, \text{ for Figure 6a,}$$

$$T_{\mathcal{G}}^*(x_1, x_2) = \begin{pmatrix} T_1^*(x_1 | x_2) \\ T_2^*(x_2) \end{pmatrix}, \text{ for Figure 6b.}$$

In that simple case, for Figure 6a, we recognize the “monotone lower triangular map,” and the “monotone upper triangular map,” for 6b. The causal graph of Figure 7, corresponds to the “monotone lower triangular map” in higher dimension. Finally, for the causal graph on the German Credit dataset of Figure 1, variables are sorted, and

$$T_{\mathcal{G}}^*(x_1, \dots, x_7) = \begin{pmatrix} T_1^*(x_1) \\ T_2^*(x_2 | x_1) \\ T_3^*(x_3 | x_1, x_2) \\ T_4^*(x_4 | x_2, x_3) \\ T_5^*(x_5 | x_1, x_2, x_4) \\ T_6^*(x_6 | x_3, x_5) \\ T_7^*(x_7 | x_1, x_4, x_5, x_6) \end{pmatrix}.$$

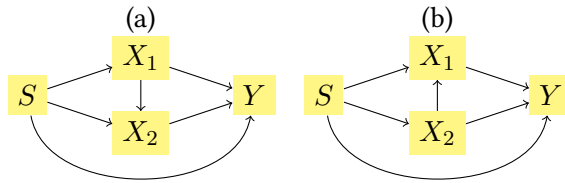


Figure 6: Two simple causal networks, with two legitimate mitigating variables, x_1 and x_2 .

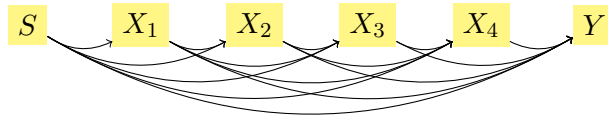


Figure 7: Causal graph associate with the “monotone lower triangular map.”

For the application on fairness in the next section, note that s is considered a “source” with no parents. Therefore, it will be possible to designate s as the first vertex in the topological ordering of the network on (s, x) . The counterfactual value will be obtained by propagating “downstream” the causal graph (following the topological order), when s changes from 0 to 1.

Algorithm 1 Sequential transport on causal graph

Require: graph \mathcal{G} on (s, \mathbf{x}) , with adjacency matrix \mathbf{A}

Require: dataset (s_i, \mathbf{x}_i) and one individual $(s = 0, \mathbf{a})$

Require: bandwidths h and b_j 's

$(s, \mathbf{v}) \leftarrow \mathbf{A}$ the topological ordering of vertices (DFS)

$T_s \leftarrow$ identity

for $j \in \mathbf{v}$ **do**

$\mathbf{p}(j) \leftarrow$ parents(j)

$T_j(\mathbf{a}_{\mathbf{p}(j)}) \leftarrow (T_{\mathbf{p}(j)_1}(\mathbf{a}_{\mathbf{p}(j)}), \dots, T_{\mathbf{p}(j)_{k_j}}(\mathbf{a}_{\mathbf{p}(j)}))$

$(\mathbf{x}_{i,j|s}, \mathbf{x}_{i,\mathbf{p}(j)|s}) \leftarrow$ subsets when $s \in \{0, 1\}$

$w_{i,j|0} \leftarrow \phi(\mathbf{x}_{i,\mathbf{p}(j)|0}; \mathbf{a}_{\mathbf{p}(j)}, \mathbf{b}_j)$ (Gaussian kernel)

$w_{i,j|1} \leftarrow \phi(\mathbf{x}_{i,\mathbf{p}(j)|1}; T_j(\mathbf{a}_{\mathbf{p}(j)}), \mathbf{b}_j)$

$\hat{f}_{h_j|s} \leftarrow$ density estimator of $x_{\cdot,j|s}$, weights $w_{\cdot,j|s}$.

$\hat{F}_{h_j|s}(\cdot) \leftarrow \int_{-\infty}^{\cdot} \hat{f}_{h_j|s}(u) du$, c.d.f.

$\hat{Q}_{h_j|s} \leftarrow \hat{F}_{h_j|s}^{-1}$, quantile

$\hat{T}_j(\cdot) \leftarrow \hat{Q}_{h_j|1} \circ \hat{F}_{h_j|0}(\cdot)$

end for

$\mathbf{a}^* \leftarrow (T_1(\mathbf{a}_1), \dots, T_d(\mathbf{a}_d))$

return $(s = 1, \mathbf{a}^*)$, counterfactual of $(s = 0, \mathbf{a})$

4.3 Algorithm

Algorithm 1 describes this sequential approach, which can be illustrated using the causal graph in Figure 6a, as shown in Figure 8. The preliminary step is to determine the topological order of the causal graph. In Figure 6a the order is $(s, (x_1, x_2))$. The first step is to estimate densities $\hat{f}_{1|s}$ of x_1 in the two groups (s being either 0 or 1) as shown in the top left of Figure 8. Next, numerical integration and inverse are used to compute the cumulative distributions $\hat{F}_{1|s}$ and quantile functions $\hat{Q}_{1|s}$. To compute the counterfactual for $(s = 0, \mathbf{a})$, a_1^* is calculated as $\hat{T}_1(a_1)$, where $\hat{T}_1(\cdot) = \hat{Q}_{1|1} \circ \hat{F}_{1|0}(\cdot)$. The second step involves considering the second variable in the topological order, conditional on its parents. Suppose x_2 is the second variable, and for illustration that x_1 is the (only) parent of x_2 . The densities $\hat{f}_{2|s}$ of x_2 are then estimated in the two groups, conditional on their parents: either conditional on $x_1 = a_1$ (subgroup $s = 0$), or conditional on $x_1 = a_1^*$ (subgroup $s = 1$). This is feasible since all transports of parents were computed in an earlier step. This can be visualized in the bottom left of Figure 8. As in the previous step, the conditional cumulative distributions $\hat{F}_{2|s}$ and conditional quantile functions $\hat{Q}_{2|s}$ (conditional on the parents) are computed. Then a_2^* is determined as $\hat{T}_2(a_2)$ where $\hat{T}_2(\cdot) = \hat{Q}_{2|1} \circ \hat{F}_{2|0}(\cdot)$. This process is repeated until all variables have been considered. At the end, starting from an individual with features $\mathbf{x} = \mathbf{a}$, in group $s = 0$, the counterfactual version in group $s = 1$ is obtained, with transported features, *mutatis mutandis*, \mathbf{a}^* .

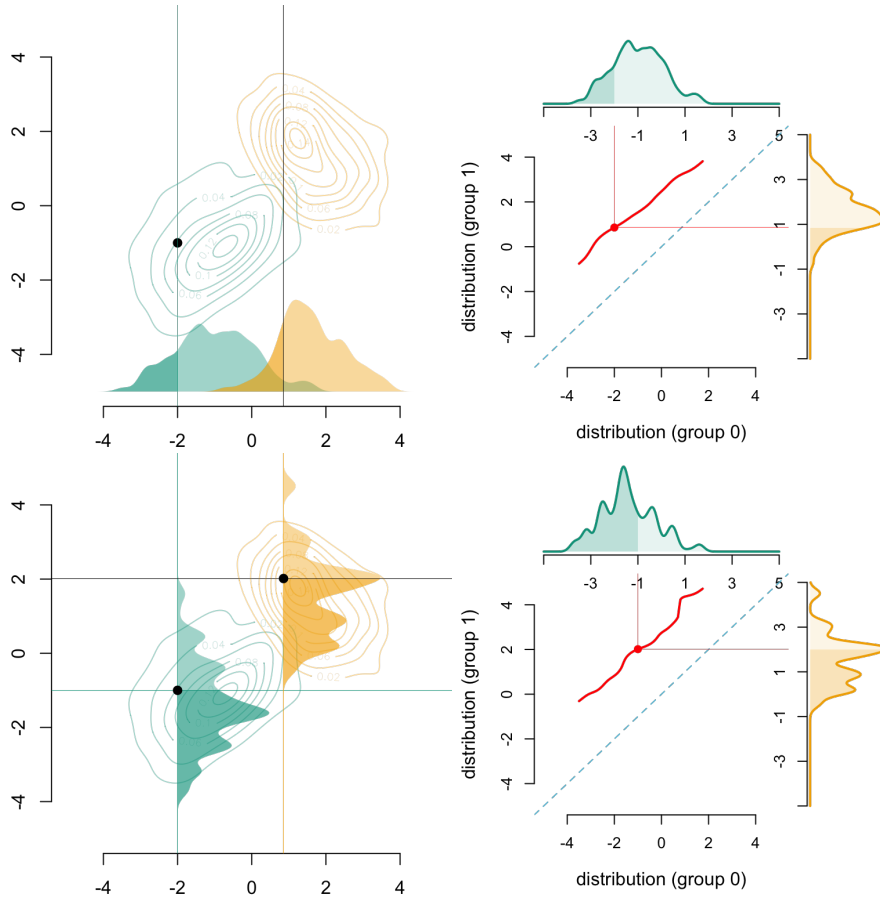


Figure 8: Illustration of Algorithm 1 for DAG in Figure 6a, with simulated data; first step at the top, second step at the bottom.

5 Interpretable Counterfactual Fairness

5.1 Individual Counterfactual Fairness

5.1.1 General Context

Following [Dwork et al. \(2012\)](#), a fair decision means that “similar individuals” are treated similarly. As discussed in the introduction, [Kusner et al. \(2017\)](#) and [Russell et al. \(2017\)](#) considered a “counterfactual fairness” criterion. Based on the approach discussed above, it is possible to quantify unfairness for a single individual of a model m , trained on features (s, \mathbf{x}) to predict an outcome y . If $y \in \{0, 1\}$ is binary, then m represents the underlying score, corresponding to the conditional probability that $y = 1$.

5.1.2 Illustration With Simulated Data

Consider the causal graphs in Figure 6, with one sensitive attribute s , two legitimate features x_1 and x_2 and one outcome y . Here, y is the score obtained from a logistic regression, specifically,

$$m(x_1, x_2, s) = \left(1 + \exp \left[- \left((x_1 + x_2)/2 + \mathbf{1}(s = 1) \right) \right] \right)^{-1}.$$

Iso-scores can be visualized at the top of Figure 9, with group 0 on the left, 1 on the right. Consider an individual $(s, x_1, x_2) = (s = 0, -2, -1)$ in group 0, with a score of 18.24% (bottom left of Figure 9). Using Algorithm 1, its counterfactual counterpart $(s = 1, x_1^*, x_2^*)$ can be

constructed. The resulting score varies depending on the causal assumption. The score would be 40.95% assuming the causal graph of Figure 6a, and 54.06% assuming causal graph 6b. In the first case, the *mutatis mutandis* difference $m(s = 1, x_1^*, x_2^*) - m(s = 0, x_1, x_2)$, i.e., +22.70%, is:

$$\begin{aligned} m(s = 1, x_1, x_2) - m(s = 0, x_1, x_2) & : -10.65\% \\ + m(s = 1, x_1^*, x_2) - m(s = 1, x_1, x_2) & : +17.99\% \\ + m(s = 1, x_1^*, x_2^*) - m(s = 1, x_1^*, x_2) & : +15.37\%. \end{aligned}$$

The first term is the *ceteris paribus* difference, the second one the change in x_1 and the third one the change in x_2 , conditional on the change in x_1 . If, instead, we assume the causal graph of Figure 6b, the score of the same individual would become 54.06% and the *mutatis mutandis* difference $m(s = 1, x_1^*, x_2^*) - m(s = 0, x_1, x_2)$, i.e., +35.82%, is:

$$\begin{aligned} m(s = 1, x_1, x_2) - m(s = 0, x_1, x_2) & : -10.66\% \\ + m(s = 1, x_1, x_2^*) - m(s = 1, x_1, x_2) & : +16.07\% \\ + m(s = 1, x_1^*, x_2^*) - m(s = 1, x_1, x_2^*) & : +30.41\%. \end{aligned}$$

At the bottom right of Figure 9, the *mutatis mutandis* impact on the scores can be visualized.

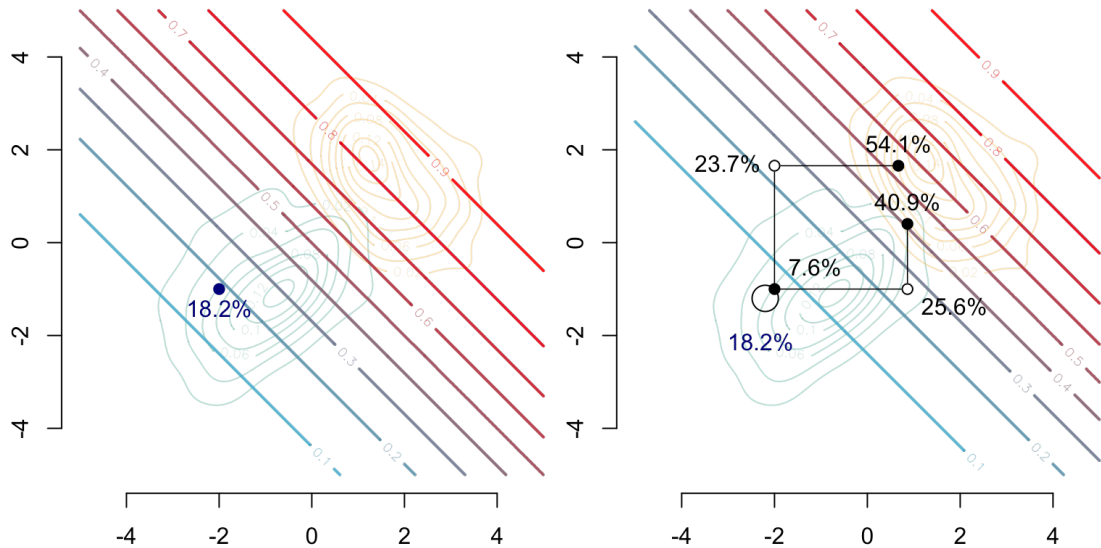


Figure 9: In the background, level curves for $(x_1, x_2) \mapsto m(0, x_1, x_2)$ and $m(1, x_1, x_2)$ respectively on the left and on the right. Then, on the left, individual $(s, x_1, x_2) = (s = 0, -2, -1)$ (predicted 18.24% by model m), and on the right, visualization of two counterfactuals $(s = 1, x_1^*, x_2^*)$ according to causal graphs 6a (bottom right path, predicted 40.94%) and 6b (top left path, predicted 54.06%).

5.2 Global Fairness Metrics

Instead of focusing on a single individual, it is possible to quantify the fairness of a model m on a global scale. For example, a counterfactual demographic parity (CDP) measure can be defined to assess the model’s fairness across the entire population. Consider the empirical version of “counterfactual fairness” in Kusner et al. (2017)

$$\text{CDP} = \frac{1}{n_0} \sum_{i \in \mathcal{D}_0} m(1, x_i^*) - m(0, x_i), \quad (3)$$

which corresponds to the “average treatment effect of the treated” in the classical causal literature. This can be computed more efficiently using Algorithm 2 in Appendix B, which offers a faster alternative compared to Algorithm 1.

6 Application on Real Data

We analyze the Law School Admission Council dataset (Wightman, 1998), focusing on four variables: race $s \in \{\text{Black}, \text{White}\}$ (corresponding to 0 and 1), undergraduate GPA before law school (x_1 , UGPA), Law School Admission Test (x_2 , LSAT), and a binary response (y) indicating whether the first-year law school grade (FYA) is above the median, as described in Black, Yeom, and Fredrikson (2020). Unlike De Lara et al. (2024); Black, Yeom, and Fredrikson (2020); Kusner et al. (2017), we assume the causal graph in Figure 10, where UGPA influences LSAT. We aim to evaluate counterfactual fairness for Black individuals in logistic regression predictions ($\hat{y}|s = 0$), comparing an “aware” classifier, i.e., that includes s among the explanatory variables, with an “unaware” model that considers only $x = (x_1, x_2)$. Fairness is measured using CDP (see Equation 3). We apply the sequential transport method from Algorithm 2 to compute counterfactuals $\hat{y}^*(s = 1)|s = 0$ following the network’s topological order in Figure 10. These results are compared with those obtained from multivariate OT (De Lara et al., 2024) and quantile regressions (Plečko, Bennett, and Meinshausen, 2021), namely *fairadapt*.

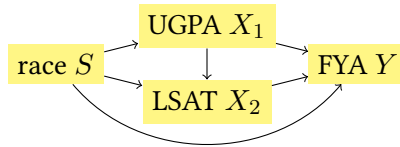


Figure 10: Causal graph of the Law dataset.

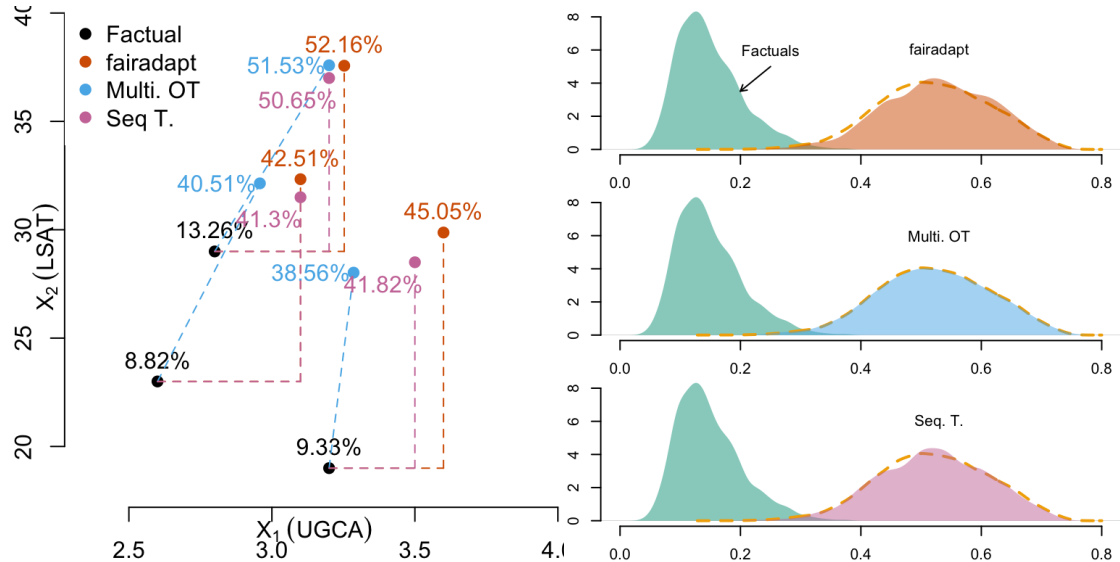


Figure 11: Counterfactual calculations for three Black individuals on the left (percentages indicate predicted scores), and densities of predicted scores (aware model) for all Black individuals with factuals and counterfactuals on the right. The dashed line represents the density of predicted scores for the observed White individuals.

	<i>fairadapt</i>	multi. OT	seq. T
Aware model	0.3810	0.3727	0.3723
Unaware model	0.1918	0.1821	0.1817

Table 1: CDP for Black individuals from Eq. 3 comparing classifier predictions over original features \mathbf{x} (resp. $(s = 0, \mathbf{x})$) and their counterfactuals \mathbf{x}^* (resp. $(s = 1, \mathbf{x}^*)$), using *fairadapt*, multivariate OT, and sequential transport.

Figure 11 illustrates the similarity between *fairadapt* and sequential transport, both assuming a DAG, as shown by the counterfactual pathways for three Black individuals (left) and the alignment of counterfactual predicted score densities (right). The density of multivariate OT counterfactuals resembles factual White outcome distribution due to its matching process. Overall, the three methods yield similar results, as reflected in the aggregated counterfactual fairness metric in Table 1. Lastly, the “aware” model, which directly incorporates s into its covariates, is less counterfactually fair than the “unaware” model.

7 Conclusion

In this paper, we propose a sequential transport approach for constructing counterfactuals based on OT theory while respecting the underlying causal graph of the data. By using conditional univariate transport maps, we derive closed-form solutions for each coordinate of an individual’s characteristics, which facilitates the interpretation of both individual counterfactual fairness of our predictive model, and global fairness through “counterfactual demographic parity.”

References

- Ahuja, R. K.; Magnanti, T. L.; and Orlin, J. B. 1993. *network flows: Theory, algorithms, and applications*. Prentice Hall.
- Ambrosio, L.; Gigli, N.; and Savaré, G. 2005. *Gradient flows: in metric spaces and in the space of probability measures*. Springer.
- Backhoff, J.; Beiglböck, M.; Lin, Y.; and Zalashko, A. 2017. Causal transport in discrete time and applications. *SIAM Journal on Optimization*, 27(4): 2528–2562.
- Barber, D. 2012. *Bayesian reasoning and machine learning*. Cambridge University Press.
- Barocas, S.; Hardt, M.; and Narayanan, A. 2023. *Fairness and machine learning: Limitations and opportunities*. MIT press.
- Bartl, D.; Beiglböck, M.; and Pammer, G. 2021. The Wasserstein space of stochastic processes. arXiv:2104.14245.
- Black, E.; Yeom, S.; and Fredrikson, M. 2020. Fliptest: fairness testing via optimal transport. In *Proceedings of the 2020 Conference on Fairness, Accountability, and Transparency*, 111–121.
- Bogachev, V. I.; Kolesnikov, A. V.; and Medvedev, K. V. 2005. Triangular transformations of measures. *Sbornik: Mathematics*, 196(3): 309.
- Bongers, S.; Forré, P.; Peters, J.; and Mooij, J. M. 2021. Foundations of structural causal models with cycles and latent variables. *The Annals of Statistics*, 49(5): 2885–2915.
- Bonnotte, N. 2013. From Knothe’s rearrangement to Brenier’s optimal transport map. *SIAM Journal on Mathematical Analysis*, 45(1): 64–87.
- Brenier, Y. 1991. Polar factorization and monotone rearrangement of vector-valued functions. *Communications on pure and applied mathematics*, 44(4): 375–417.
- Bunne, C.; Krause, A.; and Cuturi, M. 2022. Supervised training of conditional Monge maps. *Advances in Neural Information Processing Systems*, 35: 6859–6872.
- Cannon, A. J. 2018. Non-crossing nonlinear regression quantiles by monotone composite quantile re-

- gression neural network, with application to rainfall extremes. *Stochastic Environmental Research and Risk Assessment*, 32: 3207–3225.
- Carlier, G.; Galichon, A.; and Santambrogio, F. 2010. From Knothe’s transport to Brenier’s map and a continuation method for optimal transport. *SIAM Journal on Mathematical Analysis*, 41(6): 2554–2576.
- Charpentier, A.; Flachaire, E.; and Gallic, E. 2023. Optimal transport for counterfactual estimation: A method for causal inference. In *Optimal Transport Statistics for Economics and Related Topics*, 45–89. Springer.
- Cheridito, P.; and Eckstein, S. 2023. Optimal transport and Wasserstein distances for causal models. arXiv:2303.14085.
- Chernozhukov, V.; Fernández-Val, I.; and Melly, B. 2013. Inference on counterfactual distributions. *Econometrica*, 81(6): 2205–2268.
- Cordero-Erausquin, D. 2004. Non-smooth differential properties of optimal transport. *Contemporary Mathematics*, 353: 61–72.
- Cormen, T. H.; Leiserson, C. E.; Rivest, R. L.; and Stein, C. 2022. *Introduction to algorithms*. MIT press.
- De Lara, L.; González-Sanz, A.; Asher, N.; Risser, L.; and Loubes, J.-M. 2024. Transport-based counterfactual models. *Journal of Machine Learning Research*, 25(136): 1–59.
- Dempster, A. P. 1972. Covariance selection. *Biometrics*, 157–175.
- Dwork, C.; Hardt, M.; Pitassi, T.; Reingold, O.; and Zemel, R. 2012. Fairness through awareness. In *Proceedings of the 3rd innovations in theoretical computer science conference*, 214–226.
- Hallin, M.; and Konen, D. 2024. Multivariate Quantiles: Geometric and Measure-Transportation-Based Contours. arXiv:2401.02499.
- Hardt, M.; Price, E.; and Srebro, N. 2016. Equality of opportunity in supervised learning. *Advances in neural information processing systems*, 29: 3315–3323.
- Higham, N. J. 2008. *Functions of matrices: theory and computation*. SIAM.
- Hosseini, B.; Hsu, A. W.; and Taghvaei, A. 2023. Conditional Optimal Transport on Function Spaces. arXiv:2311.05672.
- Kahn, A. B. 1962. Topological sorting of large networks. *Communications of the ACM*, 5(11): 558–562.
- Kantorovich, L. V. 1942. On the translocation of masses. In *Doklady Akademii Nauk USSR*, volume 37, 199–201.
- Kearns, M.; and Roth, A. 2019. *The ethical algorithm: The science of socially aware algorithm design*. Oxford University Press.
- Kilbertus, N.; Rojas Carulla, M.; Parascandolo, G.; Hardt, M.; Janzing, D.; and Schölkopf, B. 2017. Avoiding discrimination through causal reasoning. *Advances in neural information processing systems*, 30.
- Knothe, H. 1957. Contributions to the theory of convex bodies. *Michigan Mathematical Journal*, 4(1): 39–52.
- Koenker, R. 2005. *Quantile regression*, volume 38. Cambridge university press.
- Koenker, R.; and Bassett Jr, G. 1978. Regression quantiles. *Econometrica: journal of the Econometric Society*, 33–50.
- Koenker, R.; Chernozhukov, V.; He, X.; and Peng, L. 2017. *Handbook of quantile regression*. CRC Press.
- Koller, D.; and Friedman, N. 2009. *Probabilistic graphical models: principles and techniques*. MIT press.
- Kusner, M. J.; Loftus, J.; Russell, C.; and Silva, R. 2017. Counterfactual Fairness. In Guyon, I.; Luxburg, U. V.; Bengio, S.; Wallach, H.; Fergus, R.; Vishwanathan, S.; and Garnett, R., eds., *Advances in Neural Information Processing Systems 30*, 4066–4076. NIPS.
- Lauritzen, S. L. 2020. *Lectures on graphical models*. University of Copenhagen.
- Ma, L.; and Koenker, R. 2006. Quantile regression methods for recursive structural equation models. *Journal of Econometrics*, 134(2): 471–506.
- Meinshausen, N.; and Ridgeway, G. 2006. Quantile regression forests. *Journal of machine learning research*, 7(6).
- Monge, G. 1781. Mémoire sur la théorie des déblais et des remblais. *Histoire de l’Académie Royale des Sciences de Paris*.
- Pearce, T.; Jeong, J.-H.; jia, y.; and Zhu, J. 2022. Censored Quantile Regression Neural Networks for Distribution-Free Survival Analysis. In Koyejo, S.; Mohamed, S.; Agarwal, A.; Belgrave, D.; Cho, K.; and Oh, A., eds., *Advances in Neural Information Processing Systems*, volume 35, 7450–7461. Curran Associates, Inc.
- Pearl, J. 2000. Comment. *Journal of the American Statistical Association*, 95(450): 428–431.
- Pearl, J. 2009. *Causality*. Cambridge university press.

- Pearl, J.; and Mackenzie, D. 2018. *The book of why: the new science of cause and effect*. Basic books.
- Plečko, D.; Bennett, N.; and Meinshausen, N. 2021. fairadapt: Causal reasoning for fair data pre-processing. arXiv:2110.10200.
- Plečko, D.; and Meinshausen, N. 2020. Fair data adaptation with quantile preservation. *Journal of Machine Learning Research*, 21(242): 1–44.
- Rosenblatt, M. 1952. Remarks on a multivariate transformation. *The annals of mathematical statistics*, 23(3): 470–472.
- Rubin, D. B. 2005. Causal inference using potential outcomes: Design, modeling, decisions. *Journal of the American Statistical Association*, 100(469): 322–331.
- Russell, C.; Kusner, M. J.; Loftus, J.; and Silva, R. 2017. When worlds collide: integrating different counterfactual assumptions in fairness. *Advances in neural information processing systems*, 30.
- Santambrogio, F. 2015. Optimal transport for applied mathematicians. *Birkäuser, NY*, 55(58-63): 94.
- Shpitser, I.; Richardson, T. S.; and Robins, J. M. 2022. Multivariate counterfactual systems and causal graphical models. In *Probabilistic and causal inference: The works of Judea Pearl*, 813–852. Association for Computing Machinery.
- Susser, M. 1991. What is a cause and how do we know one? A grammar for pragmatic epidemiology. *American Journal of Epidemiology*, 133(7): 635–648.
- Takatsu, A. 2011. Wasserstein geometry of Gaussian measures. *Osaka Journal of Mathematics*, 48(4): 1005–1026.
- Villani, C. 2003. *Topics in optimal transportation*, volume 58. American Mathematical Society.
- Villani, C. 2009. *Optimal transport: old and new*, volume 338. Springer.
- Watson, D. S.; Gultchin, L.; Taly, A.; and Floridi, L. 2021. Local explanations via necessity and sufficiency: Unifying theory and practice. *Uncertainty in Artificial Intelligence*, 1382–1392.
- Wightman, L. F. 1998. LSAC National Longitudinal Bar Passage Study. LSAC Research Report Series. Technical report, Law School Admission Council, Newtown, PA.
- Wright, S. 1921. Correlation and causation. *Journal of Agricultural Research*, 20.
- Wright, S. 1934. The method of path coefficients. *The annals of mathematical statistics*, 5(3): 161–215.
- Zech, J.; and Marzouk, Y. 2022a. Sparse approximation of triangular transports, part I: The finite-dimensional case. *Constructive Approximation*, 55(3): 919–986.
- Zech, J.; and Marzouk, Y. 2022b. Sparse approximation of triangular transports, part II: The infinite-dimensional case. *Constructive Approximation*, 55(3): 987–1036.

APPENDIX

A Gaussian Case

The Gaussian case is the most simple one since mapping T^* , corresponding to OT, can be expressed analytically (it will be a linear mapping). Furthermore, conditional distributions of a multivariate Gaussian distribution are Gaussian distributions, and that can be used to consider an iteration of simple conditional (univariate) transports, as a substitute to joint transport T^* . Here Φ denotes the univariate cumulative distribution function of the standard Gaussian distribution $\mathcal{N}(0, 1)$.

A.1 Univariate Optimal Gaussian Transport

One can easily prove that the optimal mapping, from a $\mathcal{N}(\mu_0, \sigma_0^2)$ to a $\mathcal{N}(\mu_1, \sigma_1^2)$ distribution is (see Figure 5):

$$x_1 = T^*(x_0) = \mu_1 + \frac{\sigma_1}{\sigma_0}(x_0 - \mu_0),$$

which is a nondecreasing linear transformation.

A.2 Multivariate Optimal Gaussian Transport

Recall that $\mathbf{X} \sim \mathcal{N}(\boldsymbol{\mu}, \boldsymbol{\Sigma})$, $\mathbf{B} = \boldsymbol{\Sigma}^{-1}$, if its density, with respect to Lebesgue measure is

$$f(\mathbf{x}) \propto \exp\left(-\frac{1}{2}(\mathbf{x} - \boldsymbol{\mu})^\top \mathbf{B} \boldsymbol{\Sigma}^{-1} (\mathbf{x} - \boldsymbol{\mu})\right). \quad (4)$$

If $\mathbf{X}_0 \sim \mathcal{N}(\boldsymbol{\mu}_0, \boldsymbol{\Sigma}_0)$ and $\mathbf{X}_1 \sim \mathcal{N}(\boldsymbol{\mu}_1, \boldsymbol{\Sigma}_1)$, the optimal mapping is also linear,

$$\mathbf{x}_1 = T^*(\mathbf{x}_0) = \boldsymbol{\mu}_1 + \mathbf{A}(\mathbf{x}_0 - \boldsymbol{\mu}_0),$$

where \mathbf{A} is a symmetric positive matrix that satisfies $\mathbf{A} \boldsymbol{\Sigma}_0 \mathbf{A} = \boldsymbol{\Sigma}_1$, which has a unique solution given by $\mathbf{A} = \boldsymbol{\Sigma}_0^{-1/2} (\boldsymbol{\Sigma}_0^{1/2} \boldsymbol{\Sigma}_1 \boldsymbol{\Sigma}_0^{1/2})^{1/2} \boldsymbol{\Sigma}_0^{-1/2}$, where $M^{1/2}$ is the square root of the square (symmetric) positive matrix M based on the Schur decomposition ($M^{1/2}$ is a positive symmetric matrix), as described in Higham (2008). If $\boldsymbol{\Sigma} = \begin{pmatrix} 1 & r \\ r & 1 \end{pmatrix}$, and if $a = \sqrt{(1 - \sqrt{1 - r^2})/2}$, then:

$$\boldsymbol{\Sigma}^{1/2} = \begin{pmatrix} \sqrt{1 - a^2} & a \\ a & \sqrt{1 - a^2} \end{pmatrix}.$$

Observe further this mapping is the gradient of the convex function

$$\psi(\mathbf{x}) = \frac{1}{2}(\mathbf{x} - \boldsymbol{\mu}_0)^\top \mathbf{A}(\mathbf{x} - \boldsymbol{\mu}_0) + \mathbf{x} - \boldsymbol{\mu}_1^\top \mathbf{x}$$

and $\nabla T^* = \mathbf{A}$ (see Takatsu (2011) for more properties of Gaussian transport). And if $\boldsymbol{\mu}_0 = \boldsymbol{\mu}_1 = \mathbf{0}$, and if $\boldsymbol{\Sigma}_0 = \mathbb{I}$ and $\boldsymbol{\Sigma}_1 = \boldsymbol{\Sigma}$, $\mathbf{x}_1 = T^*(\mathbf{x}_0) = \boldsymbol{\Sigma}^{1/2} \mathbf{x}_0$. Hence, $\boldsymbol{\Sigma}^{1/2}$ is a linear operator that maps from $\mathbf{X}_0 \sim \mathcal{N}(\mathbf{0}, \mathbb{I})$ (the reference density) to $\mathbf{X}_1 \sim \mathcal{N}(\mathbf{0}, \boldsymbol{\Sigma})$ (the target density).

A.3 Conditional Gaussian Transport

Alternatively, since $\boldsymbol{\Sigma}$ is a positive definite matrix, from the Cholesky decomposition, it can be written as the product of a lower (or upper) triangular matrix and its conjugate transpose,

$$\boldsymbol{\Sigma} = \mathbf{L} \mathbf{L}^\top = \mathbf{U}^\top \mathbf{U}.$$

Remark. If $\boldsymbol{\Sigma} = \begin{pmatrix} 1 & r \\ r & 1 \end{pmatrix}$, then $\mathbf{L} = \boldsymbol{\Sigma}_{2|1}^{1/2} = \begin{pmatrix} 1 & 0 \\ r & \sqrt{1 - r^2} \end{pmatrix}$ while $\mathbf{U} = \boldsymbol{\Sigma}_{1|2}^{1/2} = \boldsymbol{\Sigma}_{2|1}^{1/2\top} = \mathbf{L}^\top$. Then $\mathbf{L}^\top \mathbf{L} = \boldsymbol{\Sigma} = \mathbf{U}^\top \mathbf{U}$.

Both \mathbf{L} and \mathbf{U} are linear operators that map from $\mathbf{X}_0 \sim \mathcal{N}(\mathbf{0}, \mathbb{I})$ (the reference density) to $\mathbf{X}_1 \sim \mathcal{N}(\mathbf{0}, \boldsymbol{\Sigma})$ (the target density). $\mathbf{x}_0 \mapsto \mathbf{L} \mathbf{x}_0$ and $\mathbf{x}_0 \mapsto \mathbf{U} \mathbf{x}_0$ are respectively linear lower and upper triangular transport maps.

More generally, in dimension 2, consider the following (lower triangular) mapping $T(x_0, y_0) = (T_x(x_0), T_{y|x}(y_0|x_0))$,

$$\mathcal{N}\left(\begin{pmatrix} \mu_{0x} \\ \mu_{0y} \end{pmatrix}, \begin{pmatrix} \sigma_{0x}^2 & r_0 \sigma_{0x} \sigma_{0y} \\ r_0 \sigma_{0x} \sigma_{0y} & \sigma_{0y}^2 \end{pmatrix}\right) \xrightarrow{T} \mathcal{N}\left(\begin{pmatrix} \mu_{1x} \\ \mu_{1y} \end{pmatrix}, \begin{pmatrix} \sigma_{1x}^2 & r_1 \sigma_{1x} \sigma_{1y} \\ r_1 \sigma_{1x} \sigma_{1y} & \sigma_{1y}^2 \end{pmatrix}\right),$$

where $T_x(x_0)$ and $T_{y|x}(y_0|x_0)$ are respectively

$$\begin{cases} \mu_{1x} + \frac{\sigma_{1x}}{\sigma_{0x}}(x_0 - \mu_{0x}) \\ \mu_{1y} + \frac{r_1 \sigma_{1y}}{\sigma_{1x}}(T_x(x_0) - \mu_{1x}) + \sqrt{\frac{\sigma_{0x}^2(\sigma_{1y}^2 \sigma_{1x}^2 - r_1^2 \sigma_{1y}^2)}{(\sigma_{0y}^2 \sigma_{0x}^2 - r_0^2 \sigma_{0y}^2) \sigma_{1x}^2}} (y_0 - \mu_{0y} - \frac{r_0 \sigma_{0y}}{\sigma_{0x}}(x_0 - \mu_{0x})) \end{cases}$$

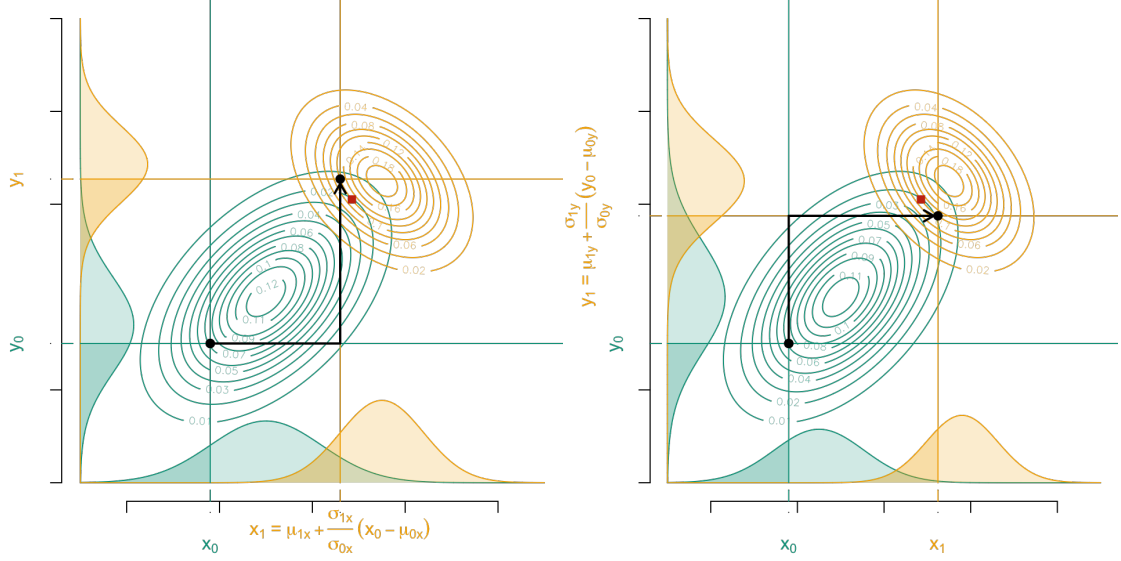


Figure 12: Two Gaussian conditional optimal transports. On the left-hand side, the process begins with a univariate transport along the x axis (using T_x^*), followed by a transport along the y axis on the conditional distributions (using $T_{y|x}^*$), corresponding to the “lower triangular affine mapping.” On the right-hand side, the sequence is reversed: it starts with a univariate transport along the y axis (using T_y^*) followed by transport along the x axis on the conditional distributions (using $T_{x|y}^*$). The red square is the multivariate OT of the point in the bottom left, corresponding to the “upper triangular affine mapping.”

that are both linear mappings. This can be visualized on the left side of Figure 12.

Of course, this is highly dependent on the axis parametrization. Instead of considering projections on the axis, one could consider transport in the direction \vec{u} , followed by transport in the direction \vec{u}^\perp (on conditional distributions). This can be visualized in Figure 13.

A.4 Gaussian Probabilistic Graphical Models

An interesting feature of the Gaussian multivariate distribution is that any marginal and any conditional distribution (given other components) is still Gaussian. More precisely, if

$$\mathbf{x} = \begin{pmatrix} x_1 \\ x_2 \end{pmatrix}, \quad \boldsymbol{\mu} = \begin{pmatrix} \mu_1 \\ \mu_2 \end{pmatrix} \quad \text{and} \quad \boldsymbol{\Sigma} = \begin{pmatrix} \Sigma_{11} & \Sigma_{12} \\ \Sigma_{21} & \Sigma_{22} \end{pmatrix},$$

then $X_1 \sim \mathcal{N}(\boldsymbol{\mu}_1, \boldsymbol{\Sigma}_{11})$, while, with notations of Eq. 4, we can also write $\mathbf{B}_1 = \mathbf{B}_{11} - \mathbf{B}_{12}\mathbf{B}_{22}^{-1}\mathbf{B}_{21}$ (based on properties of inverses of block matrices, also called the Schur complement of a block matrix). Furthermore, conditional distributions are also Gaussian, $X_1|X_2 = x_2 \sim \mathcal{N}(\boldsymbol{\mu}_{1|2}, \boldsymbol{\Sigma}_{1|2})$,

$$\begin{cases} \boldsymbol{\mu}_{1|2} = \boldsymbol{\mu}_1 + \boldsymbol{\Sigma}_{12}\boldsymbol{\Sigma}_{22}^{-1}(x_2 - \boldsymbol{\mu}_2) \\ \boldsymbol{\Sigma}_{1|2} = \boldsymbol{\Sigma}_{11} - \boldsymbol{\Sigma}_{12}\boldsymbol{\Sigma}_{22}^{-1}\boldsymbol{\Sigma}_{21}, \end{cases}$$

and the inverse of the conditional variance is simply \mathbf{B}_{11} .

It is well known that if $\mathbf{X} \sim \mathcal{N}(\boldsymbol{\mu}, \boldsymbol{\Sigma})$, $X_i \perp\!\!\!\perp X_j$ if and only if $\Sigma_{i,j} = 0$. More interestingly, we also have the following result, initiated by Dempster (1972):

Proposition A.1. *If $\mathbf{X} \sim \mathcal{N}(\boldsymbol{\mu}, \boldsymbol{\Sigma})$, with notations of Eq. 4, $\mathbf{B} = \boldsymbol{\Sigma}^{-1}$, \mathbf{X} is Markov with respect to $\mathcal{G} = (E, V)$ if and only if $B_{i,j} = 0$ whenever $(i, j), (j, i) \notin E$.*

Proof. This is a direct consequence of the following property : if $\mathbf{X} \sim \mathcal{N}(\boldsymbol{\mu}, \boldsymbol{\Sigma})$, $X_i \perp\!\!\!\perp X_j | \mathbf{X}_{-i,j}$ if and only if $B_{i,j} = 0$ (since the log-density has separate terms in x_i and x_j). \square

A.5 Sequential Transport

In the Gaussian case we obviously recover the results of Section A.3, if we plug Gaussian distributions in the expressions of Section 4,

$$\begin{cases} X_{0:1} \sim \mathcal{N}(\mu_{0:1}, \sigma_{0:1}^2), \text{ hence } F_{0:1}(x) = \Phi(\sigma_{0:1}^{-1}(x - \mu_{0:1})) \\ X_{1:1} \sim \mathcal{N}(\mu_{1:1}, \sigma_{1:1}^2), \text{ hence } F_{1:1}^{-1}(u) = \mu_{1:1} + \sigma_{1:1}\Phi^{-1}(u) \end{cases}$$

thus

$$T_1^*(x) = F_{1:1}^{-1}(F_{0:1}(x)) = \mu_{1:1} + \frac{\sigma_{1:1}}{\sigma_{0:1}}(x - \mu_{0:1}),$$

while

$$\begin{cases} X_{0:2}|x_{0:1} \sim \mathcal{N}(\mu_{0:2|1}, \sigma_{0:2|1}^2), \\ X_{1:2}|x_{0:1} \sim \mathcal{N}(\mu_{1:2|1}, \sigma_{1:2|1}^2), \end{cases}$$

i.e.,

$$\begin{cases} F_{0:2|1}(x) = \Phi(\sigma_{0:2|1}^{-1}(x - \mu_{0:2|1})), \\ F_{1:2|1}^{-1}(u) = \mu_{1:2|1} + \sigma_{1:2|1}\Phi^{-1}(u), \end{cases}$$

where we consider $X_{0:2}$ conditional to $X_{0:1} = x_{0:1}$ in the first place,

$$\begin{cases} \mu_{0:2|1} = \mu_{0:2} + \frac{\sigma_{0:2}}{\sigma_{0:1}}(x_{0:1} - \mu_{0:1}), \\ \sigma_{0:2|1}^2 = \sigma_{0:2}^2 - \frac{\sigma_{0:1}^2}{r_0^2 \sigma_{0:2}^2}, \end{cases}$$

and $X_{1:2}$ conditional to $X_{1:1} = T_1^*(x_{0:1})$ in the second place,

$$\begin{cases} \mu_{1:2|1} = \mu_{1:2} + \frac{\sigma_{1:2}}{\sigma_{1:1}}(T_1^*(x_{0:1}) - \mu_{1:1}), \\ \sigma_{1:2|1}^2 = \sigma_{1:2}^2 - \frac{\sigma_{1:1}^2}{r_1^2 \sigma_{1:2}^2}, \end{cases}$$

thus

$$T_{2|1}(x) = F_{1:2|1}^{-1}(F_{0:2|1}(x)) = \mu_{1:2|1} + \frac{\sigma_{1:2|1}}{\sigma_{0:2|1}}(x - \mu_{0:2|1}),$$

which is

$$\begin{aligned} & \mu_{1:2} + \frac{r_1 \sigma_{1:2}}{\sigma_{1:1}} \left(\mu_{1:1} + \frac{\sigma_{1:1}}{\sigma_{0:1}}(x_{0:1} - \mu_{0:1}) - \mu_{1:1} \right) \\ & + \sqrt{\frac{\sigma_{0:1}^2 (\sigma_{1:2}^2 \sigma_{1:1}^2 - r_1^2 \sigma_{1:2}^2)}{(\sigma_{0:2}^2 \sigma_{0:1}^2 - r_0^2 \sigma_{0:2}^2) \sigma_{1:1}^2}} \cdot \left(x - \mu_{0:2} - \frac{r_0 \sigma_{0:2}}{\sigma_{0:1}}(x_{0:1} - \mu_{0:1}) \right). \end{aligned}$$

A.6 General Conditional Transport

An interesting property of Gaussian vectors is the stability under rotations. In dimension 2, instead of a sequential transport of \mathbf{x} on \vec{e}_x and then (conditionally) on \vec{e}_y , one could consider a projection on any unit vector \vec{u} (with angle θ), and then (conditionally) along the orthogonal direction \vec{u}^\perp . In Figure 13, we can visualize the set of all counterfactuals \mathbf{x}^* when $\theta \in [0, 2\pi]$. The (global) optimal transport is also considered.

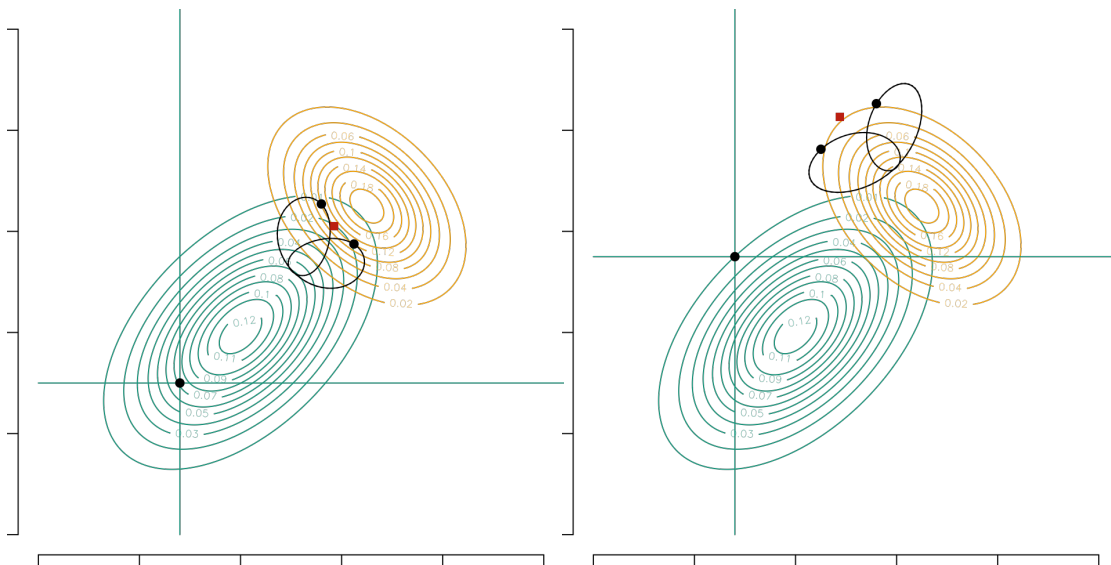


Figure 13: Gaussian conditional optimal transports. Each graph illustrates the transport starting from a different point (black point in the bottom left corner). The process begins with a univariate transport along the direction \vec{u} (using $T_{\vec{u}}^*$) followed by a transport along the orthogonal direction \vec{u}^\perp , on conditional distributions (using $T_{\vec{u}^\perp|\vec{u}}^*$). The curves in the upper right corner of each panel represent the set of all transport maps of the same point (bottom left corner) for all possible directions \vec{u} , the black points correspond to classical x (horizontal) and y (vertical) directions. The red point corresponds to the global optimal transport.

B Algorithms

While Algorithm 1 is intuitive, it becomes inefficient when computing counterfactuals for thousands of individuals, as conditional densities, c.d.f.'s and quantile functions should be computed for each individual. An alternative is to compute these quantities on a grid, store them, and then retrieve them as needed. These objects are generated using Algorithm 2 (see also Figures 14 and 15, which visualize the vectors $F_{1|0}$, $F_{1|1}$, $F_{2|0}[\cdot, i]$ and $F_{2|1}[\cdot, j]$ —with light colors corresponding to small probabilities and darker ones to large probabilities). Algorithm 3 computes the counterfactual for a given individual with $s = 0$ using the stored functions. In Algorithm 2 if j has no parents, $\text{parents}(j) = \emptyset$, $d_j = 0$ and then $F_{j|s}$ and $Q_{j|s}$ are vectors (of length k). In Algorithm 3, in that case, $\mathbf{i}_0 = \mathbf{i}_1 = \emptyset$.

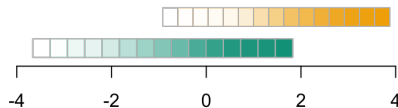


Figure 14: Visualization of vectors $F_{1|0}$ (below) and $F_{1|1}$ (on top) for the example of Figure 8, with $k = 15$.

Algorithm 2 Faster sequential transport on causal graph (1)

Require: graph on (s, \mathbf{x}) , with adjacency matrix \mathbf{A}
Require: dataset (s_i, \mathbf{x}_i) and $k \in \mathbb{N}$ some grid size,
Require: grids $\mathbf{g}_{j|s} = (g_{j,1|s}, \dots, g_{j,k|s})$, for all variable j
Require: grid $\mathbf{u} = (1, \dots, k)/(k+1)$, for all j
 $(s, \mathbf{v}) \leftarrow \mathbf{A}$ the topological ordering of vertices (DFS)
for $j \in \mathbf{v}$ **do**
 $\mathbf{p}(j) \leftarrow \text{parents}(j)$, dimension d_j
 $\mathcal{G}_{j|s} \leftarrow \text{grid } \mathbf{g}_{\mathbf{p}(j)_1|s} \times \dots \times \mathbf{g}_{\mathbf{p}(j)_{d_j}|s}$
 $F_{j|s} \leftarrow \text{tensors } k \times k^{d_j}$, taking values in \mathbf{u}
 $Q_{j|s} \leftarrow \text{tensors } k \times k^{d_j}$, taking values in $\mathbf{g}_{j|s}$
 for $\mathbf{i} = (i_1, \dots, i_{d_j}) \in \{1, \dots, k\}^{d_j}$ **do**
 $F_{j|s}[\cdot, \mathbf{i}] \leftarrow \text{c.d.f. of } X_j | \mathbf{X}_{\mathbf{p}(j)} = \mathbf{g}_{\mathbf{i}|s}, S = s$
 $Q_{j|s}[\cdot, \mathbf{i}] \leftarrow \text{quantile of } X_j | \mathbf{X}_{\mathbf{p}(j)} = \mathbf{g}_{\mathbf{i}|s}, S = s$
 end for
end for

Algorithm 3 Faster sequential transport on causal graph (2)

Require: $F_{1|s}, \dots, F_{d|s}$ and $Q_{d|s}, \dots, Q_{1|s}$ (algorithm 2)
Require: grids $\mathbf{g}_{1|s}, \dots, \mathbf{g}_{d|s}, \mathcal{G}_{1|s}, \dots, \mathcal{G}_{d|s}$ and \mathbf{u}
Require: features $\mathbf{a} \in \mathbb{R}^d$ (group 0)
 $\mathbf{b} \leftarrow \mathbf{a}$
for $j \in \mathbf{v}$ **do**
 $\mathbf{i}_0 \leftarrow \mathbf{a}_{\mathbf{p}(j)}$ on grid $\mathcal{G}_{j|0}$
 $k_0 \leftarrow a_j$ on grid $\mathbf{g}_{j|0}$
 $p \leftarrow F_{j|0}[k_0, \mathbf{i}_0]$
 $\mathbf{i}_1 \leftarrow \mathbf{b}_{\mathbf{p}(j)}$ on grid $\mathcal{G}_{j|1}$
 $k_1 \leftarrow p$ on grid \mathbf{u}
 $b_j \leftarrow Q_{j|1}[k_1, \mathbf{i}_1]$
end for
return \mathbf{b} (counterfactual in group 1)

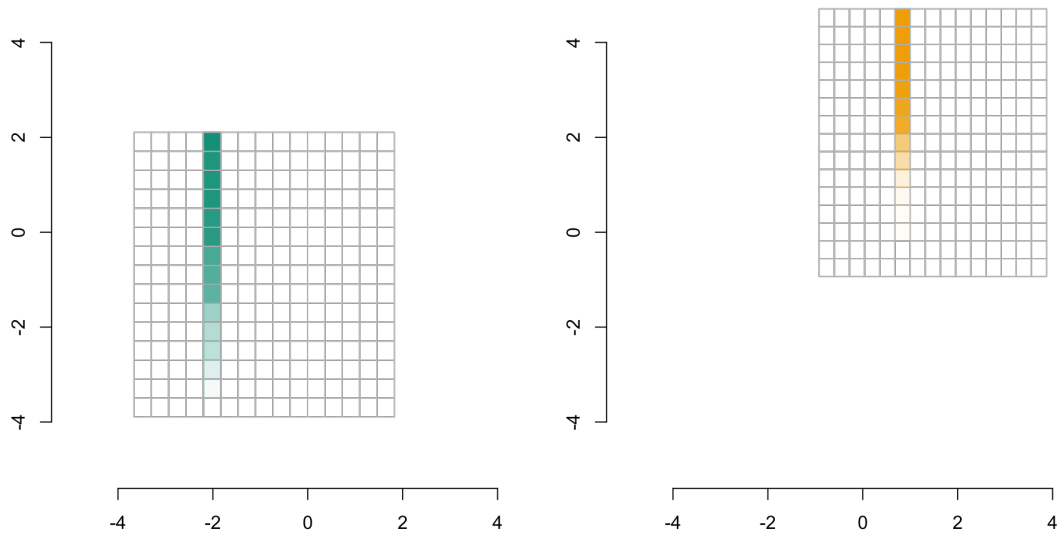


Figure 15: Visualization of matrices $F_{2|0}$ (on the left) and $F_{2|1}$ (on the right) for the example of Figure 8, with $k = 15$. Vertical vectors are $F_{2|0}[\cdot, i]$ and $F_{2|1}[\cdot, j]$.